VIP Nanofabrication

DOI: 10.1002/anie.201204609

Self-Assembly of Vertically Aligned Gold Nanorod Arrays on Patterned Substrates**

*Thibaut Thai, Yuanhui Zheng, Soon Hock Ng, Stephen Mudie, Matteo Altissimo, and Udo Bach**

Metal nanoparticles show unique optical properties that have become a major focal point in photonic research. The interaction of these nanostructures with light gives rise to a collective movement of the metal's free electron cloud in resonance with the incident electromagnetic field, known as surface plasmons.[1] Surface plasmons are strongly confined to the close vicinity of these metal structures, such that photonic energy is localized to dimensions well below the diffraction limit. This effect can be exploited for a number of applications such as sensing,[2] computing,[3] solar energy conversion,[4] and nanolithography.[5,6]

Bottom-up approaches take advantage of self-assembly processes to construct complex plasmonic nanostructures from individual metal nanoparticle building blocks. The latter can be readily synthesized with controlled sizes and shapes through chemistry routes.[7] The use of building blocks with anisotropic shapes, such as metal nanorods, adds an additional level of complexity and presents both an exciting opportunity for the realization of novel functional nanostructures, and a significant challenge towards their controlled assembly. The optical properties of gold nanorods (GNRs) are highly sensitive to their aspect ratio, allowing their plasmon absorption to be tuned throughout the visible well into the IR range.[8] Within assemblies of GNRs, the plasmonic coupling between adjacent GNRs provides an additional means to tailor their optical properties.[9,10] Rod-shaped building blocks can therefore be used to fabricate more elaborate structures such as arrays of vertically aligned nanorods.[11] Standing arrays of GNRs unlock new potential applications such as surface-enhanced Raman spectroscopy (SERS),[12] plasmonic metamaterials for biosensing,[13] cavity resonators,[14] nanoscale light polarizers,[15] and ultrafast nonlinear optics.[16] They can form spontaneously upon drying of a GNR solution on a substrate. A number of techniques have been reported[17–22] that aim to control this assembly by exchanging the ligand and then drop-casting the modified GNR solution on a surface. Using this strategy, Zhang et al.[23] observed the formation of domains of standing nanorods on patterned substrates, yet it proved difficult to achieve high assembly yields and good control over the confinement of these arrays. Lately, Ng et al.[24] have described the synthesis of free-standing superlattice sheets consisting of a monolayer of standing nanorods. Based on these studies, capillary forces and convective flows appear to play a crucial role in the formation of standing arrays of GNRs. Denkov et al.[25] were the first to describe the formation of two-dimensional crystals upon evaporation of a colloidal solution. At the three-phase contact line of the solution, attractive capillary forces promote packing of adjacent particles that can be described as a nucleus formation.[26] Convective flow resulting from solvent evaporation draws more particles toward the contact line leading to crystal growth. Several groups have applied this concept at the nanoscale with various templates to create more elaborate nanostructures. For instance, Cui et al.[27] have demonstrated the integration of spherical and tetrapod-shaped nanoparticles into lithographically patterned devices with single-particle resolution. Recently, Kuemin et al.[28] have achieved the oriented assembly of individual GNRs into prefabricated surface patterns, with GNRs aligned parallel to the substrate surface. Capillary assembly has proven its remarkable potential to control the placement of anisotropic nanoparticles, yet the precise spatial arrangement of vertical arrays of GNRs still remains a challenge.

Herein we describe a technique based on capillary and convective assembly for the self-assembly of GNRs exclusively to standing arrays with precise placement. The GNR assembly process employed here is illustrated in Scheme 1. To produce the template, a silica-coated silicon wafer has been patterned through conventional photolithography with a periodic set of 2 μm × 2 μm gold squares, with a 6 μm center-to-center distance (see the Supporting Information). The surface properties of the gold on silica template are controlled first with a UV–ozone treatment then a silanization step. The UV–ozone treatment enhances the hydrophilic character of the gold surface,[29] while the subsequent silanization step is selective to the silica surface, increasing its hydrophobic character. The wettability contrast of surfaces has been shown

[*] T. Thai, Dr. Y. H. Zheng, S. H. Ng, Prof. U. Bach
Department of Materials Engineering, Monash University
Wellington Road, Clayton, Victoria 3800 (Australia)
E-mail: udo.bach@monash.edu
Homepage: http://www.udobach.com
T. Thai, Dr. Y. H. Zheng, S. H. Ng, Dr. M. Altissimo, Prof. U. Bach
The Melbourne Centre for Nanofabrication
151 Wellington road, Clayton, Victoria 3168 (Australia)
Prof. U. Bach
CSIRO, Materials Science and Engineering Clayton South,
Victoria 3169 (Australia)
Dr. S. Mudie
The Australian Synchroton
800 Blackburn Road, Clayton, Victoria 3168 (Australia)

[**] We acknowledge financial support from the Australian Research Council through an Australian Research Fellowship (U.B.). Further financial support has been received from Commonwealth Scientific and Industrial Research Organization through an OCE Science Leader position (U.B.). This work was performed in part at the Melbourne Centre for Nanofabrication, an initiative partly funded by the Commonwealth of Australia and the Victorian government.

Supporting information for this article is available on the WWW under http://dx.doi.org/10.1002/anie.201204609.

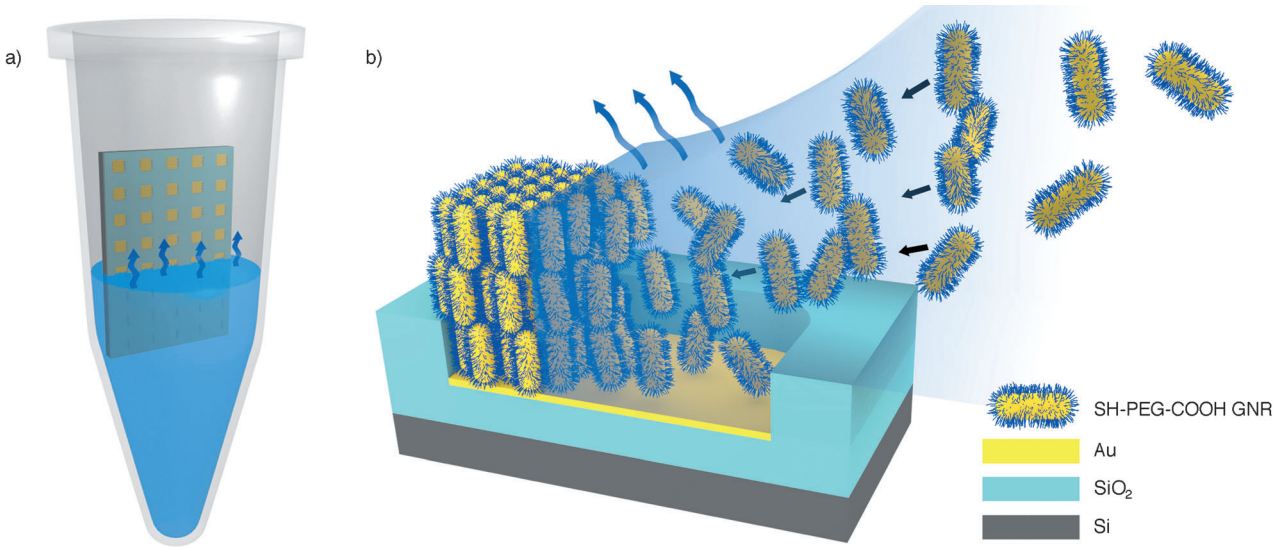

Scheme 1. a) Illustration of the experimental setup. The micropatterned substrate is placed in the center of an Eppendorf tube and immersed in a concentrated colloidal solution of GNRs. The substrate is left to dry under isothermal conditions. b) Schematic representation of the formation of standing arrays of GNRs on a template upon solvent evaporation.

to direct the growth of colloidal crystals in a site-selective manner.[30,31] Furthermore the recessed features of the gold patterns used here provides a spatial confinement for the crystallization of nanorods. The template is immersed in an open Eppendorf tube containing an aqueous GNR solution. It is placed vertically in the center of the tube and the solution is then left to dry at a controlled temperature. As the solvent evaporates, the meniscus of the solution slowly recedes down the substrate's surface toward the bottom of the tube.

The formation of vertical aligned nanorods onto predefined areas is critically dependent on the interaction energy between the rods and the substrate, as well as between neighboring rods.[23] The surface functionalization of GNRs therefore plays a crucial role in predisposing their self-assembly properties. In the present work, nanorods were modified with thiol-PEG-carboxyl ($SH\text{-}C_{11}H_{22}(OCH_2CH_2)_6\text{-}OCH_2\text{-}COOH$). Our group has shown in a recent study[32] that spherical nanoparticles modified with this ligand self-assemble into ordered hexagonal close-packed (hcp) arrays. The ordered packing could be explained by dominant van der Waals forces and a possible interdigitation of the ligand shell present around the nanoparticles.[33–35]

SEM images of the micropattern prior to and following the successful GNR assembly are shown in Figure 1. The rounded corners of the $2\,\mu m \times 2\,\mu m$ gold micropatterns (Figure 1a inset) result from edge diffraction during the photolithography step. The step height between the recessed gold patterns and the silica surface was adjusted to 55 nm by controlling the SiO_2 etching depth and gold layer thickness (see Figure S1 in the Supporting Information). The SEM analysis reveals the successful assembly of GNRs into standing arrays, vertically aligned with respect to the surface of the substrate. The self-assembly process was achieved efficiently with a good reproducibility over large areas (Figure 1a). Remarkably, the GNR arrays are confined to isolated areas that successfully preserve the original shape of the template.

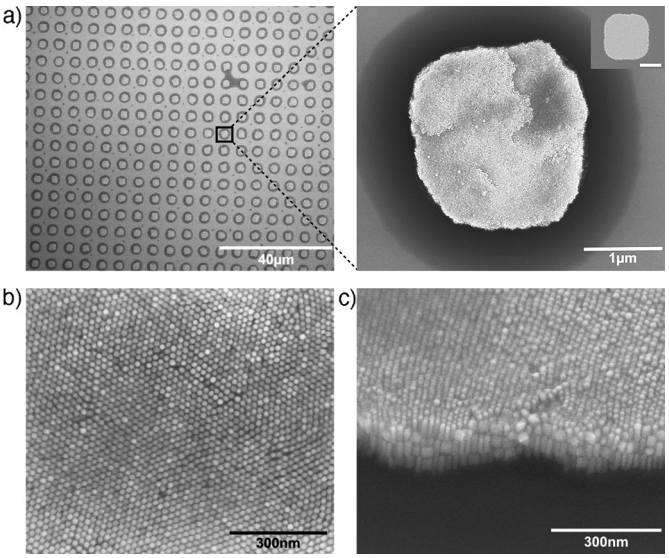

Figure 1. SEM images of self-assembled standing arrays of GNRs on a micropatterned substrate grown from a 9 nM solution at a temperature of 45 °C. a) Low-magnification image of GNR arrays and a close-up image of one individual pattern after self-assembly. The inset shows one micropattern before assembly. b) High-resolution SEM image of a GNR array. c) SEM image recorded at a tilt angle of 52°.

High-resolution SEM images show a highly ordered hcp structure of vertically aligned nanorods (Figure 1b). SEM images recorded at a tilted angle reveal that each GNR structure consists of three to four layers of densely packed arrays of standing GNRs (Figure 1c). The formation of multilayer colloidal crystals has been described by Fustin et al.[31] The directional crystallization refers to a "funnel and filter" mechanism. In this model, a strong concentration gradient induces the precrystallization of the GNRs near the contact line of the solution, before they are dragged to the crystal front by convection flow.

We have identified two main parameters that control not only the quality of the packing of these vertical arrays but also their confinement to the template, namely the concentration of the colloidal solution and its temperature. The first parameter plays a crucial role in the hcp ordering (see Figure S2 in the Supporting Information). When the solution's concentration is too low, the assemblies start to lose their close packing and display cracks throughout the arrays, leading to gaps that are filled with GNRs in random orientations. Secondly, we determined that the solution temperature controls the confinement of the arrays in the micropatterns as well as the shape variation from one nanostructure to another (see Figure S3 in the Supporting Information). The formation of free-standing GNR arrays outside the gold micropattern areas could not be observed in these experiments. This is most likely a result of the low interaction energy of the GNRs with the passivated silica surface, which impedes the nucleation of GNR arrays. However, once GNR arrays have formed on the gold micropatterns, they can act as nucleation centers for the growth of these arrays beyond the boundaries defined by the gold micropattern. This "overgrowth" can particularly be observed at low temperatures, where the lower thermal energy of the system allows the energetically less favorable growth of GNR arrays onto the silica surfaces, adjacent to the gold patterns. Increasing the solution temperature from 21 to 45 °C results in the increasing confinement of the GNR array to the actual gold templates. At temperatures above 45 °C, the arrays' shape is highly irregular and micropatterns are filled with a random number of incomplete nanorod layers.

We analyzed our nanostructures after GNR self-assembly by using small-angle X-ray scattering (SAXS) as shown in Figure 2. To collect precise data on the spatial ordering of the nanorod arrays, substrates were placed such that the short axis of the nanorod is orthogonal to the X-ray beam. These measurements were taken at the SAXS beamline at the Australian Synchrotron. The peak positions are consistent with a two-dimensional hexagonal structure with a lattice parameter of (21.69 ± 0.01) nm (see the Supporting Information). The interparticle gap extracted from the electron density map was (5 ± 1) nm, consistent with the thickness of the ligand film reported previously.[36] The presence of higher order peaks beyond 0.1 $Å^{-1}$ indicates good hcp ordering over a long range. The X-ray beam sampled approximately 750 micropatterned squares. The diffraction pattern (Figure 2 inset) shows continuous rings, implying that there is no preferred orientation of the hexagonal structures. A minor peak at 0.014 $Å^{-1}$ (and a harmonic at 0.028 $Å^{-1}$), labeled A and A2 in Figure 2, is not explained by a two-dimensional hcp structure. The correlation length of 45 nm for this peak agrees well with the length of the rods. This is indicative of a small fraction of the rods being arranged perpendicular to the beam in an end-to-end fashion. We plan future SAXS measurements using a rotation stage to tilt the samples and explore the effect on these peaks.

GNR arrays constitute excellent SERS substrates owing to their large density of interparticle gaps. Modeling of the electric field enhancement within GNR arrays[37] showed a strong dependence of the enhancement factor on the interparticle gap. The high performance of GNR arrays as SERS substrates can be explained by a nanoantenna effect that increases plasmon enhancement on the top layer.[12] To demonstrate the SERS activity of our GNR arrays we have used them as substrates for the sensing of thiolbenzene as a model analyte. All substrates were first exposed to a UV–ozone to remove thiol-PEG-carboxyl or any other organic residues and then immersed in a 1 μM solution of thiolbenzene in ethanol overnight prior to the sensing experiment. For each SERS measurement the Raman probe laser ($\lambda = 782$ nm) was focused onto the substrate surface (1 μm spot size) and aligned with the center of a GNR micropattern. The 6 μm pitch of the micropatterns was chosen such that it was possible to probe the SERS sensitivity of individual micropatterns. For comparison the SERS activity of a commercial SERS substrate (Klarite) was also tested. Two typical SERS spectra are shown in Figure 3. Both exhibit the typical fingerprint of thiolbenzene[38] with Raman peaks detectable at 417, 691, 999, 1022, 1073, and 1573 cm^{-1}. The good correlation of the peak ratios indicates similar absorption geometries for both substrates. Remarkably, the spectra show that the peak intensity on the GNR template is amplified up to 36 times, compared to

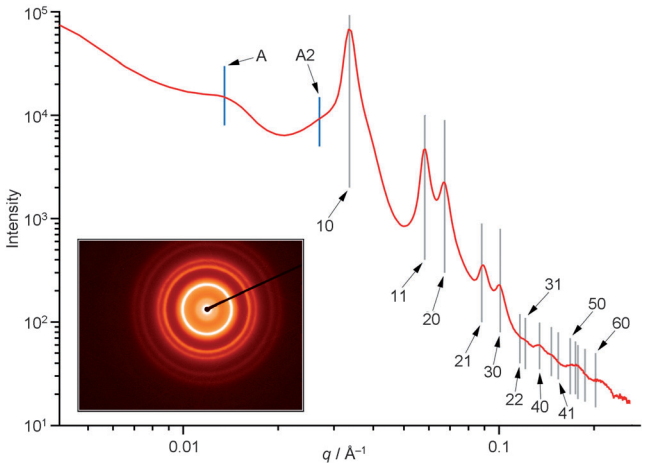

Figure 2. Transmission SAXS pattern recorded on a 100 μm × 250 μm section. Gray lines indicate the positions of hcp reflections (labels are Miller indices (hk) for the reflections; not all are shown for clarity). The inset shows the associated diffraction pattern.

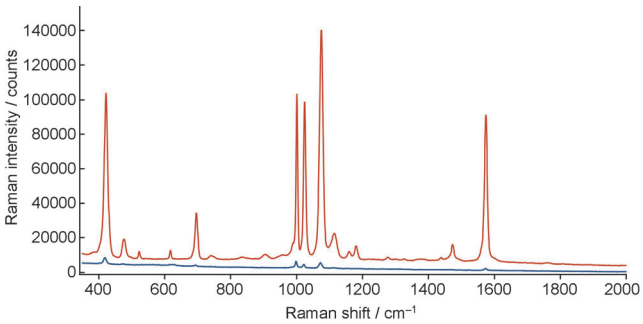

Figure 3. Raman spectra measured on the surface of GNR arrays confined to one individual micropatterned square (red) and commercial Klarite SERS (blue) substrates exposed to a 1 μM solution of thiolbenzene; excitation at 782 nm (1.15 mW).

the commercial SERS substrate. Furthermore additional peaks characteristic for thiolbenzene (616, 1155, 1182, and 1475 cm^{-1}) can clearly be identified on the GNR template but remain unresolved in the spectra recorded on the Klarite substrates. This clearly shows the exciting potential of bottom-up assembly techniques to produce nanostructures with properties that are superior to those fabricated by conventional top-down techniques.

In summary, we have introduced a reproducible and reliable GNR self-assembly strategy to produce discrete arrays of standing GNRs with hcp order onto predefined locations. Our novel fabrication strategy involves the use of capillary and convective forces and addresses two major challenges in the design of metamaterials: 1) controlling the orientation of anisotropic materials in their assemblies and 2) directing the assembly of these building blocks to predefined areas. The control over these two criteria enables the integration of highly ordered nanoparticle arrays into functional devices. This represents an important step towards the exploitation of new nanomaterials and the superior properties of their bottom-up assemblies in everyday devices. To illustrate this potential we have produced a microarray of vertically aligned GNR areas that can be addressed individually in a SERS sensing experiment. When thiolbenzene was used as a model analyte, the hcp-ordered GNR arrays showed a SERS activity up to 36 times that of the commercial Klarite SERS substrate. Controlling the interparticle and particle–substrate forces is the key towards the successful assembly of patterned arrays. These forces are mainly governed by the self-assembled monolayers of molecules that have been crafted onto the building blocks and surfaces. By further tailoring the structure and properties of these surface-active compounds it should be possible to gain further control over the self-assembly process, making it possible to control the assembly growth down to the nanometer domain, while also fine-tuning the interparticle gaps, a parameter that largely defines the SERS activities of GNR arrays.

Received: June 13, 2012
Published online: July 29, 2012

Keywords: anisotropy · nanoparticles · nanostructures · Raman spectroscopy · self-assembly

[1] M. Pelton, J. Aizpurua, G. Bryant, *Laser Photonics Rev.* **2008**, *2*, 136 – 159.
[2] M. E. Stewart, C. R. Anderton, L. B. Thompson, J. Maria, S. K. Gray, J. A. Rogers, R. G. Nuzzo, *Chem. Rev.* **2008**, *108*, 494 – 521.
[3] S. A. Maier, P. G. Kik, H. A. Atwater, S. Meltzer, E. Harel, B. E. Koel, A. A. G. Requicha, *Nat. Mater.* **2003**, *2*, 229 – 232.
[4] V. E. Ferry, J. N. Munday, H. A. Atwater, *Adv. Mater.* **2010**, *22*, 4794 – 4808.
[5] P. G. Kik, A. L. Martin, S. A. Maier, H. A. Atwater, *Proc. Soc. Photo-Opt. Instrum. Eng.* **2002**, *4810*, 7 – 13.
[6] A. Sundaramurthy, P. J. Schuck, N. R. Conley, D. P. Fromm, G. S. Kino, W. E. Moerner, *Nano Lett.* **2006**, *6*, 355 – 360.
[7] M. Grzelczak, J. Pérez-Juste, P. Mulvaney, L. M. Liz-Marzán, *Chem. Soc. Rev.* **2008**, *37*, 1783 – 1791.
[8] X. Huang, S. Neretina, M. A. El-Sayed, *Adv. Mater.* **2009**, *21*, 4880 – 4910.
[9] P. K. Jain, S. Eustis, M. A. El-Sayed, *J. Phys. Chem. B* **2006**, *110*, 18243 – 18253.
[10] A. M. Funston, C. Novo, T. J. Davis, P. Mulvaney, *Nano Lett.* **2009**, *9*, 1651 – 1658.
[11] S. Ahmed, K. M. Ryan, *Nano Lett.* **2007**, *7*, 2480 – 2485.
[12] R. A. Alvarez-Puebla, et al., *Proc. Natl. Acad. Sci. USA* **2011**, *108*, 8157 – 8161.
[13] A. V. Kabashin, P. Evans, S. Pastkovsky, W. Hendren, G. A. Wurtz, R. Atkinson, R. Pollard, V. A. Podolskiy, A. V. Zayats, *Nat. Mater.* **2009**, *8*, 867 – 871.
[14] D. P. Lyvers, J. Moon, A. V. Kildishev, V. M. Shalaev, A. Wei, *ACS Nano* **2008**, *2*, 2569 – 2576.
[15] R. Kullock, W. R. Hendren, A. Hille, S. Grafström, P. R. Evans, R. J. Pollard, R. Atkinson, L. M. Eng, *Opt. Express* **2008**, *16*, 21671 – 21681.
[16] G. A. Wurtz, R. Pollard, W. Hendren, G. P. Wiederrecht, D. J. Gosztola, V. A. Podolskiy, A. V. Zayats, *Nat. Nanotechnol.* **2011**, *6*, 107 – 111.
[17] K. Mitamura, T. Imae, N. Saito, O. Takai, *J. Phys. Chem. B* **2007**, *111*, 8891 – 8898.
[18] H. Nakashima, K. Furukawa, Y. Kashimura, K. Torimitsu, *Langmuir* **2008**, *24*, 5654 – 5658.
[19] T. S. Sreeprasad, A. K. Samal, T. Pradeep, *Langmuir* **2008**, *24*, 4589 – 4599.
[20] A. Guerrero-Martínez, J. Pérez-Juste, E. Carbó-Argibay, G. Tardajos, L. M. Liz-Marzán, *Angew. Chem.* **2009**, *121*, 9648 – 9652; *Angew. Chem. Int. Ed.* **2009**, *48*, 9484 – 9488.
[21] Y. Xie, S. Guo, Y. Ji, C. Guo, X. Liu, Z. Chen, X. Wu, Q. Liu, *Langmuir* **2011**, *27*, 11394 – 11400.
[22] A. Petukhova, J. Greener, K. Liu, D. Nykypanchuk, R. Nicolaÿ, K. Matyjaszewski, E. Kumacheva, *Small* **2012**, *8*, 731 – 737.
[23] X. Zhang, T. Imae, *J. Phys. Chem. C* **2009**, *113*, 5947 – 5951.
[24] K. C. Ng, I. B. Udagedara, I. D. Rukhlenko, Y. Chen, Y. Tang, M. Premaratne, W. Cheng, *ACS Nano* **2012**, *6*, 925 – 934.
[25] N. D. Denkov, O. D. Velev, P. A. Kralchevsky, I. B. Ivanov, H. Yoshimura, K. Nagayama, *Langmuir* **1992**, *8*, 3183 – 3190.
[26] N. D. Denkov, O. D. Velev, P. A. Kralchevsky, I. B. Ivanov, H. Yoshimura, K. Nagayama, *Nature* **1993**, *361*, 26.
[27] Y. Cui, M. T. Björk, J. A. Liddle, C. Sönnichsen, B. Boussert, A. P. Alivisatos, *Nano Lett.* **2004**, *4*, 1093 – 1098.
[28] C. Kuemin, L. Nowack, L. Bozano, N. D. Spencer, H. Wolf, *Adv. Funct. Mater.* **2012**, *22*, 702 – 708.
[29] D. E. King, *J. Vac. Sci. Technol. A* **1995**, *13*, 1247 – 1253.
[30] C. A. Fustin, G. Glasser, H. W. Spiess, U. Jonas, *Adv. Mater.* **2003**, *15*, 1025.
[31] C. Fustin, G. Glasser, H. W. Spiess, U. Jonas, *Langmuir* **2004**, *20*, 9114 – 9123.
[32] Y. Zheng, C. H. Lalander, U. Bach, *Chem. Commun.* **2010**, *46*, 7963 – 7965.
[33] S. Liu, T. Zhu, R. Hu, Z. Liu, *Phys. Chem. Chem. Phys.* **2002**, *4*, 6059 – 6062.
[34] J. C. Love, L. A. Estroff, J. K. Kriebel, R. G. Nuzzo, G. M. Whitesides, *Chem. Rev.* **2005**, *105*, 1103 – 1169.
[35] K. J. M. Bishop, C. E. Wilmer, S. Soh, B. A. Grzybowski, *Small* **2009**, *5*, 1600 – 1630.
[36] M. R. Jones, R. J. Macfarlane, A. E. Prigodich, P. C. Patel, C. A. Mirkin, *J. Am. Chem. Soc.* **2011**, *133*, 18865 – 18869.
[37] M. D. Doherty, A. Murphy, J. McPhillips, R. J. Pollard, P. Dawson, *J. Phys. Chem. C* **2010**, *114*, 19913 – 19919.
[38] T. Joo, M. Kim, K. Kim, *J. Raman Spectrosc.* **1987**, *18*, 57 – 60.

